J Solid State Electrochem (2011) 15:125–138
DOI 10.1007/s10008-010-1074-0

ORIGINAL PAPER

Electrochemical performance of Mg–9Al–1Zn alloy in aqueous medium

Fakiha El-Taib Heakal · M. Ziad Fatayerji

Received: 16 January 2010 / Revised: 5 March 2010 / Accepted: 6 April 2010 / Published online: 30 April 2010

Abstract A systematic study on the corrosion and passivation behavior of AZ91D alloy in relation to the influence of concentration, temperature, pH, and immersion time was made in aqueous sulfate solution using electrochemical techniques including open-circuit potential, potentiodynamic polarization and impedance spectroscopy. It was found that the corrosion and pitting potentials (E_{corr} and E_{pit}) of the alloy drift to more active values with increasing either concentration (0.01–1.0 M) or temperature (278–338 K) of the test solution, suggesting that sulfate solution enhances the alloy dissolution, particularly at higher temperatures. On the other hand, values of the total film resistance (R_T) indicate that neutral solution (pH 7.0) supports the formation of a better protective layer on AZ91D surface than alkaline (pH 12.5) or acidic (pH 1.0) medium. The growth of a protective film on the alloy surface at short immersion times (up to ~50 h) is evinced by a rapid positive evolution of E_{corr} and fast decrease in the corrosion rate (i_{corr}). However, for a long-term exposure (up to 500 h) E_{corr} drifts negatively and i_{corr} increases due to breakdown of the protective film, which causes a decrease in the alloy stability. Fitting the impedance data to equivalent circuit models suitable to each behavior assisted to explore the mechanism for the attack of the sample surface at various testing times. The results obtained from the three studied electrochemical techniques are in good agreement.

Keywords AZ91D alloy · Sulfate · Concentration · Temperature · pH · EIS

F. E.-T. Heakal (✉) · M. Z. Fatayerji
Chemistry Department, Faculty of Science, Cairo University, Giza 12613, Egypt
e-mail: fakihaheakal@yahoo.com

Introduction

Over the past few decades, magnesium alloys due to their low density, high specific strength, and relative abundance have become candidate materials for many applications in microelectronics and in the automotive and aerospace industries [1]. These alloys have also good castability and damping capacity. Furthermore, reduction in the total weight of a vehicle can save fuel consumption and hence reduces environmental pollution. The most common diecast alloy is AZ91D with 9 wt.% Al content. The combination of fluidity, strength, and ductility is undeniable one of the reasons AZ91D wide spread usage. It is also ideal for the most casting components of intricate shapes, and thus eliminating the requirement of welding or bolting [2]. Nevertheless, the potential use of AZ91D alloy in several fields is limited by its poor corrosion resistance; therefore more work on its overall electrochemical traits is needed to extend its current uses wherever weight reduction is important.

It is known that AZ91D alloy contains in its microstructure the primary α-Mg grains with 2.7 wt.% Al, and surrounded by the β-eutectic phase with 7.0 wt.% Al and the large intermetallic ($Mg_{17}Al_{12}$) β-phase particles having the highest Al content (28 wt.%) [3, 4]. This heterogeneous microstructure is behind the high corrosion vulnerability of the alloy in many environments. Once a Mg-based alloy is exposed to the atmosphere, it will form an oxide film, which makes a barrier for further oxidation of the metal. However, the oxide (MgO) layer on Mg and its alloys is porous and non-protective as a result of its low Pilling–Bedworth ratio of less than unity (being 0.81 for MgO [5]). This quasi- (or limited) passivity causes poor pitting resistance for pure Mg and its alloys in presence of pitting active agents [6–11]. In sulfate solution, the surface film

formed on Mg and Mg alloys were found to be mainly composed of $Mg(OH)_2$ and/or MgO that grew rapidly during open-circuit exposure and became thicker with time [7, 12–14]. The protective action of these films is dependent on anodic or cathodic polarization where the latter affording better protection [12], as they suffered local breakdown under anodic polarization [7]. Chen et al. [3, 13] reported that for the as-cast AZ91D alloy in 0.1 M Na_2SO_4 solution, due to dissolution of α-Mg with immersion time Al ion concentration in solution increased and $MgAl_2(SO_4)_4{\cdot}2H_2O$ particles started to precipitate at the primary α-Mg areas and gradually spread to the eutectic α-Mg area and β-phase. On the other hand, Baril et al. [4, 15] indicated that at short immersion times, the oxide layer properties are essentially controlled by the MgO (or $Mg(OH)_2$) component. While at longer immersion times, the oxide layer properties become more predominantly determined by the properties of the alumina (Al_2O_3) component, whose passivating characteristics are greater than those of $Mg(OH)_2$.

Recent studies [16, 17] have indicated that AZ91D alloy exhibits a dissolution effect in acidic phosphate as well as chloride, bromide, and iodide solutions; but it is resistant to alkaline phosphate and fluoride media. In sulfate solution, however, previous studies dealt mainly with the effect of immersion time on the modifications of the corrosion product on AZ91D surface. The present results in addition address the effect of concentration, temperature and pH using the results of open-circuit potential, potentiodynamic polarization and EIS measurements, aiming for a better understanding the corrosion and passivation behavior of the alloy in this mildly aggressive medium.

Experimental

Sample of die cast alloy (AZ91D) in the form of a plate (200×100×5 mm) donated from GMN, Laval University, Canada, with a chemical composition in wt.% of: 9.0 Al, 0.67 Zn, 0.33 Mn, 0.03 Cu, 0.01 Si, 0.005 Fe, 0.002 Ni, 0.0008 Be and the reminder Mg, was used for preparing the working electrodes as described elsewhere [17]. The electrodes with a fixed surface area of 0.2 cm^2 were polished successively using finer grades of emery papers ranging from 600 to 1,500, and then rubbed with a soft cloth to obtain a silvery bright finish, degreased in acetone, washed with distilled water and dried in air at room temperature.

Measurements were made in sodium sulfate solutions prepared from (Analar-grade reagents) and triple distilled water with different concentrations in the domain 0.01–1.0 M. The pH for acidic and basic solutions was adjusted by adding few drops of H_2SO_4 or NaOH to the working solutions. A conventional three-electrode electrolytic cell was used and provided in its middle compartment with a large platinum electrode (20×40 mm) facing the working electrode for the impedance measurements. For polarization, a coiled platinum wire counter electrode was placed in a separate compartment connected to the cell via fritted glass disk. An electrochemical workstation IM6e (Zahner-elektrik, GmbH, Kronach, Germany) controlled by personal computer was used as a measuring instrument for dc and ac techniques. Cathodic and anodic polarization curves were recorded at 1 mV s^{-1} scanning rate. Electrochemical impedance spectra (EIS) were probed out at the free immersion potential using a sine wave of 10 mV amplitude while the frequency varied from 100 kHz down to 0.1 Hz. The potentials were all measured and referred against a saturated calomel electrode (SCE). Unless otherwise stated, experiments were conducted without stirring or deaeration at room temperature of 298±0.2 K inside an air thermostat.

Results and discussion

Open-circuit potential measurements

Effect of SO_4^{2-} concentration

The free immersion potential of AZ91D alloy was followed over 2 h in serial Na_2SO_4 concentrations (0.01–1.0 M), until a quasi-steady value (E_{st}) was achieved. Figure 1 shows that in the low concentration range (≤0.05 M) the potential moves positively with a decreased rate to reach E_{st}, indicating spontaneous growth of the native oxide film which has a protective ability to temporary passivate the alloy in solution [16]. In slightly concentrated (>0.05 M) sulfate solutions, the potential assumes an initial partial ennobling lasted for few minutes, and gradually drifts negatively to attain the quasi-steady value. In all solutions,

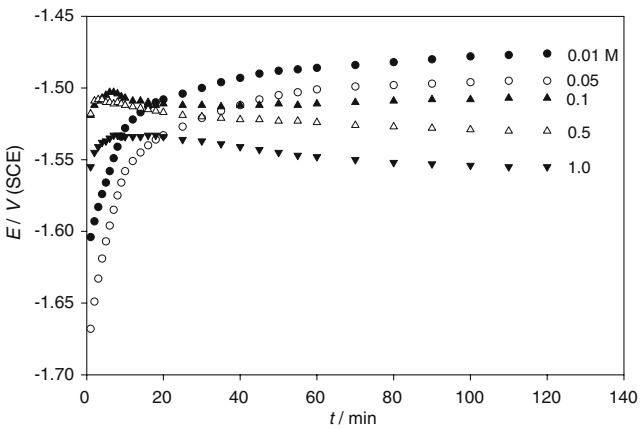

Fig. 1 Variation with time of OCP (vs. SCE) for AZ91D alloy in Na_2SO_4 solutions of different concentrations at 298 K

E_{st} is nobler in 0.01 M Na_2SO_4 solution and becomes more active with concentration, indicating instability of the corrosion product film in the solution. The plot of E_{st} against log [SO_4^{2-}] gives a straight line with a slope of −32 mV decade^{-1}, which is consistent with a reaction of Mg metal and/or $Mg(OH)_2$ film with SO_4^{2-} anions to give the easily soluble and thermodynamically stable $MgSO_4$ salt (ΔG_f^o= −1,170.6 kJ mol^{-1}). It is also noted that after a hold time of 2 h there was an increase in pH of the medium from the neutral value to pH ~10.5, which is compatible with the solubility product of $Mg(OH)_2$. Previously, using ellipsometric analysis, Hara et al. [7] reported that protective surface film mainly composed of $Mg(OH)_2$ grew under open-circuit exposure of AZ31 and AZ91D alloys to neutral 0.1 M Na_2SO_4 solution. Thereby, as corrosion proceeds, the metal surface experiences a local pH increase due to formation of $Mg(OH)_2$, whose equilibrium pH is approximately 11. The protection supplied by this film is therefore highly dependent upon the conditions of exposure.

Effect of temperature

The influence of temperature in the range 278–338 K on the stability of spontaneously formed surface film on AZ91D alloy was established in 0.1 M Na_2SO_4 using potential measurements. The OCP transient of the alloy exhibits similar trends at 318 and 338 K, where the potential shifts negatively before achieving the quasi-steady value, while at 298 K it shifts to less negative then to more negative values until reaching the E_{st} value. On the other hand, at 278 K, the electrode potential drifts positively with time from the moment of immersion, quickly at first then slowly till attaining its E_{st} value. Figure 2 reveals that E_{st} decreases rather linearly with temperature, indicating that film dissolution–formation process is shifted more towards dissolution at higher temperature and the corrosion process is cathodically controlled.

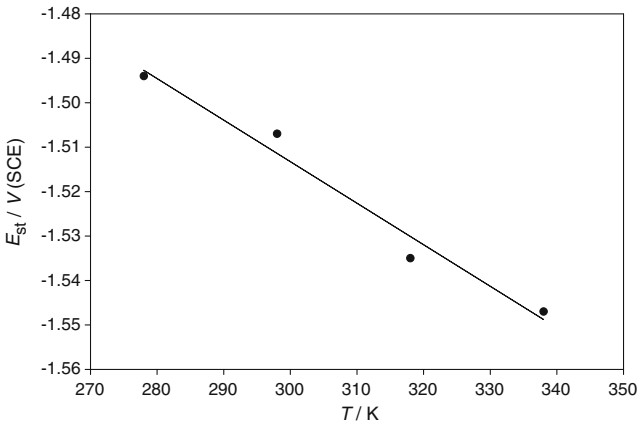

Fig. 2 Dependence of the steady potential (E_{st} vs. SCE) of AZ91D alloy on the solution temperature after 2 h immersion in 0.1 M Na_2SO_4

Effect of pH

Electrochemical measurements were also performed in aerated stagnant 0.1 M Na_2SO_4 solution of various selected pH values: 1.0, 7.0 and 12.5. According to the potential–pH diagrams [18] for Mg–H_2O and Al–H_2O systems, the immunity region of Mg is located at very low potentials (more negative than −2.60 V (SCE)) and both Mg^+ and Mg^{2+} ions appear to be the dissolution products below pH 11. On the other hand, Al is in the passive state at around neutral conditions (pH~4–8), and dissolves actively at very acidic or alkaline conditions, as it transfers to AlO_2^- anions at around pH 11, contrary to the behavior of magnesium. The OCP transients of AZ91D alloy at the chosen pH values was found to be of three types depending on the mode of their variation before achieving the quasi-stationary state. Thus, at pH 1.0 the potential is initially close to that for Mg electrode (−1.635 V) and exhibits a sharp rise to a nobler value of −1.515 V after 8 min, then it decreases rather gradually till reaching the E_{st} value of −1.570 V within 70 min. In the neutral solution (pH 7.0) the potential exhibits a small change to less negative then to more negative values before it reaches the E_{st} value of −1.505 V after only 20 min from immersion. While in the alkaline solution (pH 12.5), there is a remarkable drift in the electrode potential toward more negative values from the moment of immersion, followed by a less rapid decrease and then increases positively until it attains its E_{st} value of −1.545 V after longer time of more than 100 min. The results indicate that sulfate solution supports the formation of a spontaneous protective film on AZ91D alloy, which has a more noble, i.e., less active potential in neutral than in alkaline and acidic media.

Electrochemical impedance behavior

Effect of SO_4^{2-} concentration

EIS provides a very useful non-destructive technique for the in situ characterization of stability and modification of the corrosion product films grown on Mg and its alloys in electrolytic solutions [3, 8, 15–17]. After a 2-h immersion, the electrode impedance (|Z|) and the phase shift (Φ) were recorded and presented as Bode plots in Fig. 3a. The spectra are all characterized by a capacitive contribution at medium frequencies (MF). The corrosive nature of sulfate ions is inferred from the observed decrease in the alloy impedance with increase in its concentration, indicating corrosion promotion. This is further clarified from the monotonic decrease in the diameters of the depressed

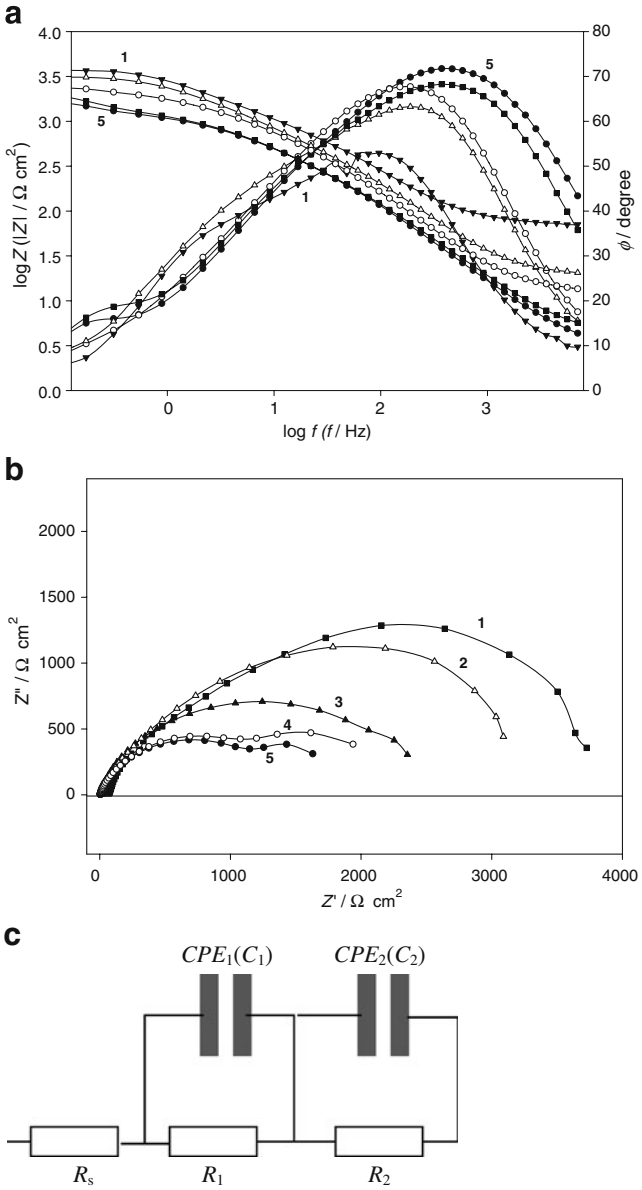

Fig. 3 EIS data of AZ91D alloy after 2 h immersion in Na_2SO_4 solutions with different concentrations: (*1*) 0.01 M, (*2*) 0.05 M, (*3*) 0.1 M, (*4*) 0.5 M, and (*5*) 1.0 M. **a** The Bode plots, **b** the Nyquist plots, and **c** The equivalent circuit used for data analysis

capacitive semicircles of the Nyquist plots (cf. Fig. 3b), which is closely related to the corrosion rate. The behavior suggests a continuous decrease in the protective efficacy of the surface film to passivate the alloy due to a decrease in its stability. Basically, in the intermediate frequency range, $|Z|$ and Φ are determined by the capacitive properties of the interface, where for ideal behavior the slope of log $|Z|$–log f relation should be −1, and the maximum in Φ–log f plot should be 90° when R_s=0. Nevertheless, the present results reveal a progressive increase in the slope from −0.335 to −0.745 with increasing concentration, meanwhile Φ_{max} is minimum (53°) in 0.01 M solution and increases gradually to 72° in 1.0 M Na_2SO_4 with a continuous shift to higher frequencies. Such anomalous behavior was reported [17] in Cl^-, Br^-, and I^- solutions, and is likely attributed to an increase in the amount of charge densities in the interface region with increasing SO_4^{2-} concentration. This leads to subsequent increase in the capacitive nature of the system while decreasing its total resistance [8]. Practically, the SO_4^{2-} anions can effectively deteriorate the alloy surface through forming the fairly soluble $MgSO_4$ salt by attacking the active anodic sites on locations with no surface film or imperfections in the partially protective film via the following reactions:

$$Mg + SO_4^{2-} \rightleftarrows MgSO_4 + 2e \quad (1)$$

$$Mg(OH)_2 + SO_4^{2-} \rightleftarrows MgSO_4 + 2OH^- \quad (2)$$

Computer simulation of EIS diagrams was performed using Thales software provided with the measuring workstation, in order to establish which equivalent circuit (EC) correlate well the results. According to ac circuit theory, an impedance plot obtained for a given electrochemical system can correlate well with the results of one or more ECs, where a successful model would be the one which gives a reasonable fit using the minimum amounts of circuit components. Within the studied concentration range, the experimentally obtained impedance data of AZ91D were found to best fit the proposed two time constants model shown in Fig. 3c, in which two constant-phase elements replace the two ideal capacitors. The model consists from the solution resistance (R_s) in series connection with two parallel combinations pairs (R_1C_{CPE1}) and (R_2C_{CPE2}) series connected [14, 16, 17]. The time constant (R_1C_{CPE1}) at high frequencies (HF) is originated from the faradaic (charge transfer) reaction and film effect across its outer layer, while the one (R_2C_{CPE2}) at low frequencies (LF) is related to contribution from the inner layer of the surface film. More confirmation for this model can be drawn from the appearance of one phase maximum at MF and another one as a shoulder at LF in the Bode plots, and also two scarcely merged semicircles in the Nyquist plots (Fig. 3a, b). In this respect, the spontaneous corrosion product film on AZ91D can be represented by a duplex layer [8, 16, 17], indicating a change in modifications of the surface film. Generally, the CPEs have been widely used to account for deviation brought about by surface roughness due to corrosion, resulting in surface inhomogeneities on the microscopic level and static disorder such as porosity [19, 20]. The frequency independent constant (Q_o) of the CPE will be equal to the idealized capacitance (C) at ω=1, ω being the angular frequency ($\omega=2\pi f$ rad s^{-1}), in accordance to the relation: $(j\,\omega)^{-1}/C=(j\,\omega)^{-\alpha}/Q_o$. Where $j^2=-1$ and the

exponent α has a value of 0.5 for a porous electrode and +1 for an ideal flat one [21], while for real polished surface, α is less than 1 and the lower the value the rougher the electrode.

Based on the above model (Fig. 3c), the calculated EC parameters for AZ91D in sulfate solutions are listed in Table 1. A change in the capacitance (C) can be used as an indicator for a change in the film thickness [16, 17, 22] following the relation: $C = A\varepsilon_o\varepsilon_r/d$, where A is the area, ε_o and ε_r are the dielectric constants of vacuum and film, respectively. Generally, the results of Table 1 reveal that the inner layer of the surface film is always thinner and more resistive than its outer layer as $C_2 > C_1$ and $R_2 > R_1$ due to the compact nature of the former one. However, the resistances and thicknesses of both layers diminish with increasing sulfate concentration. Figure 4 shows high correlation between the variation of the total film resistance ($R_T = R_1 + R_2$) and its total relative thickness ($1/C_T = 1/C_1 + 1/C_2$), where the two parameters decrease rapidly at first with concentration up to 0.1 M, then slowly till acquiring quasi-steady values at concentrations >0.5 M. Hence, the decrease in R_T value indicates corrosion promotion and thinning of the partially protective film on the alloy as the corrosiveness of SO_4^{2-} ions is increased. The dissolution of the film continues till reaching a quasi-steady state thickness at concentrations above 0.5 M, which can sustain an electric field necessary to establish a dissolution–precipitation equilibrium [17].

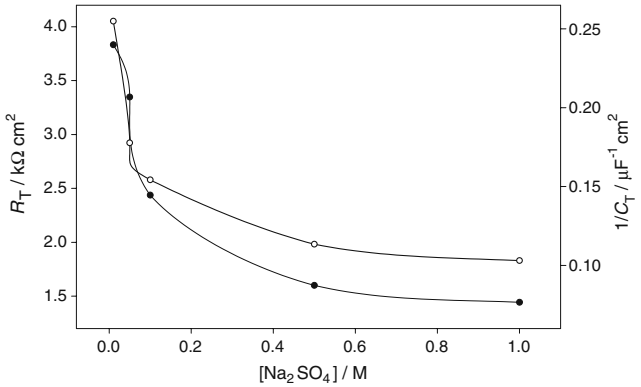

Fig. 4 The total resistance (R_T) and the relative total thickness ($1/C_T$) of the surface films on AZ91D alloy after 2 h immersion in Na_2SO_4 solutions with different concentrations

Effect of temperature

Impedance spectra of AZ91D recorded in 0.1 M Na_2SO_4 solution over the temperature range 278–338 K were analyzed using the same model shown in Fig. 3c and the circuit parameters are presented in Table 2. The overall features of the impedance diagrams remain similar, while the absolute impedance $|Z|$ and Φ_{max} decrease continuously with temperature. It can be seen that although the outer layer of the surface film is thicker than its innermost layer ($C_1 < C_2$), yet it is more porous since R_1 is much smaller than R_2, especially at lower temperatures. However, the difference between the two resistance values gradually diminishes with raising solution temperature. Figure 5 manifests that each of the two parameters R_T and $1/C_T$ of the alloy decreases with raising ambient temperature, reflecting progressive reduction in the surface film stability due to thermal activation until a quasi-steady state is attained. This means that at higher temperatures AZ91D alloy is more susceptible to corrosion attack in aqueous sulfate medium. Therefore, the results reveal that lowering solution temperature favors the formation of a thicker corrosion product film affording better protection to the alloy.

Effect of pH

The experimental impedance data measured after 2 h from electrode immersion in 0.1 M Na_2SO_4 solution of various pH are presented in Fig. 6 as Bode and Nyquist plots. The values of both impedance and phase shift of Fig. 6a, as well as the diameter of the merged depressed semicircles of Fig. 6b are all lower at pH 1.0 and higher at pH 7.0 than those at pH 12.5. Furthermore, at MF Φ_{max} shifts towards a higher frequency range following the pH order: 1.0>12.5>7.0, indicating more enhanced corrosion attack for the alloy at pH 1.0 and 12.5 as compared to the neutral solution. As previously reported [15], the present impedance responses indicate that the surface film on AZ91D comprises a thin dense MgO inner layer and a thick amorphous porous outer layer mainly composed of $Mg(OH)_2$. Like most metals and

Table 1 Equivalent circuit and corrosion parameters of AZ91D alloy immersed for 2 h in Na_2SO_4 solutions of different concentrations

[SO_4^{2-}] (M)	R_s (Ω cm^2)	R_1 (Ω cm^2)	C_1 (μF cm^{-2})	R_2 (kΩ cm^2)	C_2 (μF cm^{-2})	i_{corr} (μA cm^{-2})	E_{corr} (V)	E_{pit} (V)
0.01	66.6	642	6.3	3.19	10.50	7.80	−1.48	−0.92
0.05	17.9	584	11.4	2.76	11.07	8.31	−1.50	−0.95
0.1	11.7	535	11.4	1.90	15.01	8.50	−1.51	−0.97
0.5	3.35	514	10.6	1.09	53.35	20.2	−1.53	−1.02
1.0	2.22	498	11.6	0.95	59.75	24.8	−1.56	−1.06

i_{corr} values were obtained from Tafel extrapolation method of the cathodic log I–E curves

Table 2 Equivalent circuit and corrosion parameters of AZ91D alloy immersed for 2 h in 0.1 M Na_2SO_4 solution at various temperatures

T (K)	R_s (Ω cm^2)	R_1 (Ω cm^2)	C_1 (μF cm^{-2})	R_2 (kΩ cm^2)	C_2 (μF cm^{-2})	i_{corr} (μA cm^{-2})	E_{corr} (V)	E_{pit} (V)
278	12.7	602	11.0	4.59	14.4	3.7	−1.49	−0.90
298	11.7	535	11.9	1.90	15.0	8.5	−1.51	−0.97
318	8.6	576	13.9	0.93	57.9	21	−1.54	−1.13
338	5.2	258	14.4	0.33	61.0	29	−1.55	−1.17

i_{corr} values were obtained from Tafel extrapolation method of the cathodic log I–E curves

alloys, pure Mg and Mg alloys spontaneously form oxide or hydroxide in air and water, but the stability of this surface film is extremely low except in alkaline solutions [9, 16]. In the presence of aggressive SO_4^{2-} anions, dissolution of Mg hydroxide film occurs and corrosion can take place at a very high rate. The simplest possible reaction sequence for the formation of magnesium hydroxide layers may be as follows:

$$2Mg \rightleftarrows 2Mg^{+} + 2e \quad (3a)$$

$$2Mg^{+} + 2H_2O \rightleftarrows Mg^{2+} + Mg(OH)_2 + H_2 \quad (3b)$$

or

$$Mg^{+} \rightleftarrows Mg^{2+} + e \quad (4a)$$

$$Mg^{2} + 2H_2O + 2e \rightleftarrows Mg(OH)_2 + H_2 \quad (4b)$$

In neutral salt solutions, $Mg(OH)_2$ is predicted to be thermodynamically more stable than MgO [18]. The hydrogen bubbles nucleate and are periodically released from the surface, which becomes gray and rough in appearance with time. The ion flux and the electron transfer properties through the films determine the corrosion rate.

Simulation of the impedance data using the EC in Fig. 3c gave the best fit and the obtained circuit parameters

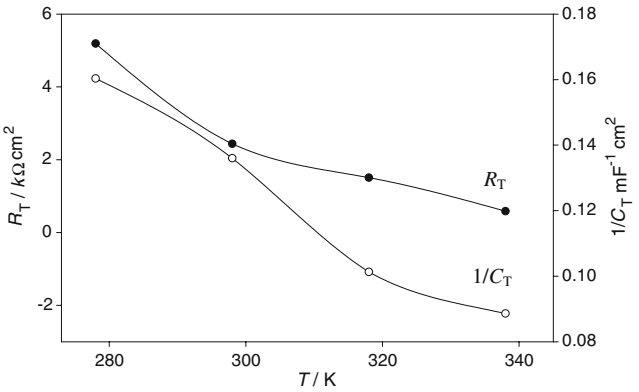

Fig. 5 The total resistance (R_T) of the surface film on AZ91D alloy and its relative thickness ($1/C_T$), after a 2-h immersion in 0.1 M Na_2SO_4 solution as a function of temperature

are listed in Table 3. As can be seen the resistance R_2 at all pH values is always much higher than R_1, thereby the inner layer controls the rate of charge-transfer reaction during the alloy corrosion in sulfate solution [23]. Moreover, Fig. 7 shows that depending on the tested pH the relative thickness of the inner layer ($1/C_2$), may have values higher (at pH 1.0), with similar value (at pH 7.0) or lower (at pH 12.5) relative to the outer layer thickness ($1/C_1$). Thus, in acidic solutions, magnesium corrodes very rapidly by evolving hydrogen with no tendency for hydroxide layer formation, since at these conditions both Mg and Al are in their active dissolution states. On the other hand, in neutral solution, the two major constituents of AZ91D alloy are passive; hence there is equal tendency for forming the oxide or hydroxide layers. However, increasing solution pH to 12.5 could speed up transformation of MgO in the barrier layer to $Mg(OH)_2$, that can explain the higher thickness of the outer layer in alkaline solution as compared to the inner. Due to the higher Pilling–Bedworth of $Mg(OH)_2$ of 1.77 [5], the resulting volume expansion at the base of the porous layer could, in turn, cause further cracking of the porous layer leading to decrease its resistance (R_1=151 Ω cm^2), despite that the outer layer thickness is significantly higher than in neutral solution, where it has a remarkable resistance (R_1) of 535 Ω cm^2.

Effect of testing time

The EIS data of AZ91D samples collected over 500 h exposures in sulfate solutions of fixed concentration can be grouped into three categories based on their behavior with the testing time. For short exposure periods (15 min–3 h) the fast evolution of layers on the alloy implies that the corrosion product film exhibits improved resistance with the lapse of time, thus leading to better alloy stability. However, at intermediate testing times (6–48 h), more corrosion products stifle the reaction and the increase in the magnitude of $|Z|$ at LF becomes very small and Φ_{max} achieves an almost constant value between 67.7° and 62.7°. However, for longer exposure periods (100–500 h), typical Bode plots in Fig. 8a reveal significant decrease in both $|Z|$ and Φ_{max} values with immersion. All Bode diagrams recorded at various immersion times demonstrate the

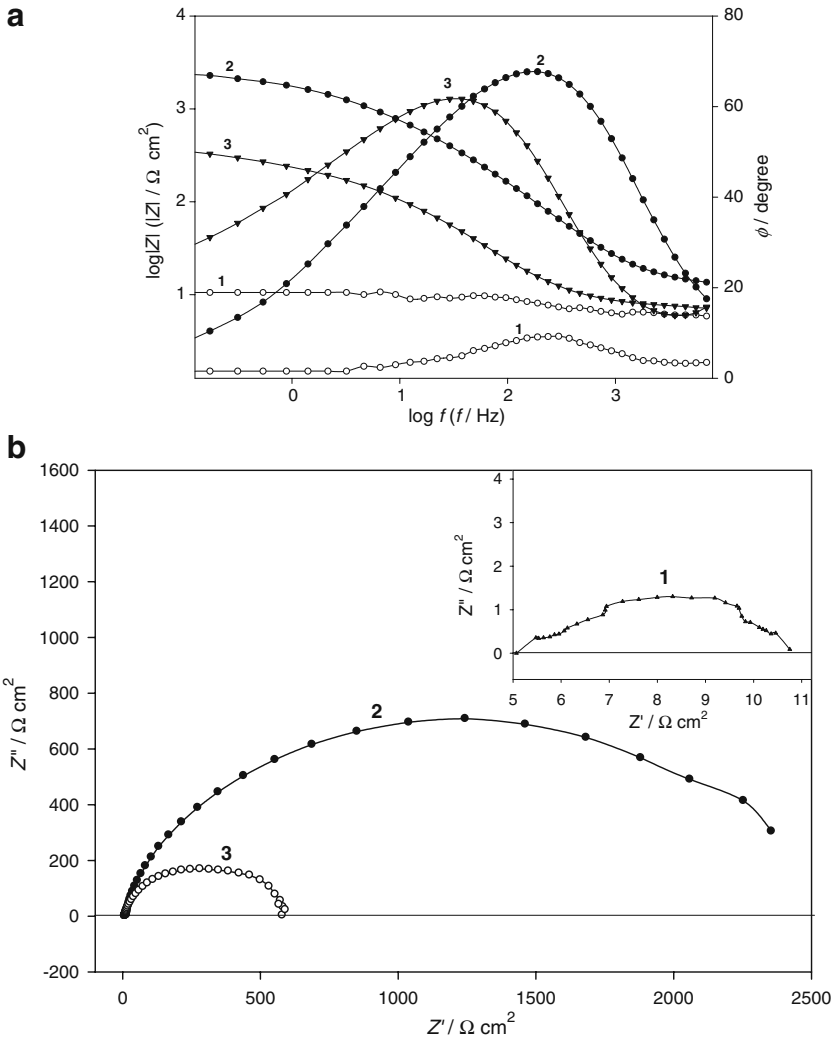

Fig. 6 EIS data of AZ91D alloy exposed for 2 h to 0.1 M Na_2SO_4 solution of various pH: (*1*) 1.0, (*2*) 7.0, and (*3*) 12.5. **a** The Bode plots, and **b** the Nyquist plots

presence of two phase lags. The main one is located at the MF region and the second appears at the LF region, which becomes clearly obvious especially when the sample was not immersed very long. On the other hand, for prolonged exposed samples the LF phase lag is no longer perceived because of the gradual shift of the MF main phase lag to lower frequencies with time. As can be seen from the typical Nyquist set in Fig. 8b, at long immersion term, the HF and MF loops are scarcely defined as they merge into an extended depressed semicircle whose diameter tends to decrease with time. This diameter is very similar to the sum of those for the two loops appearing at HF and MF ranges. Based on these considerations, the EC model shown in Fig. 3c can explain the behavior of the impedance responses at short exposure, where the impedance trend is to increase with time and the alloy surface is attacked by a uniform corrosion. The calculated equivalent circuit parameters are presented in Table 4a, where the total film resistance R_f is given by the sum R_1+R_2, and its relative thickness is denoted $1/C_f$.

At long immersion term (approximately greater than 50 h), another structure for a circuit model was used to

Table 3 Equivalent circuit parameters and corrosion parameters of AZ91D alloy immersed for 2 h in 0.1 M Na_2SO_4 solution at various pH

pH	R_s (Ω cm^2)	R_1 (Ω cm^2)	C_1 (μF cm^{-2})	R_2 (kΩ cm^2)	C_2 (μF cm^{-2})	i_{corr} (μA cm^{-2})	E_{corr} (V)	E_{pit} (V)	i_p (μA cm^{-2})
1.0	3.0	2.0	67.4	18	29.7	3700	−1.63	−1.40	2921
7.0	12.0	535	14.4	1902	15.0	8.5	−1.51	−0.97	50.6
12.5	7.0	151	7.1	402	20.4	52.5	−1.53	0.92	0.24

i_{corr} values were obtained from Tafel extrapolation method of the cathodic log *I*–*E* curves

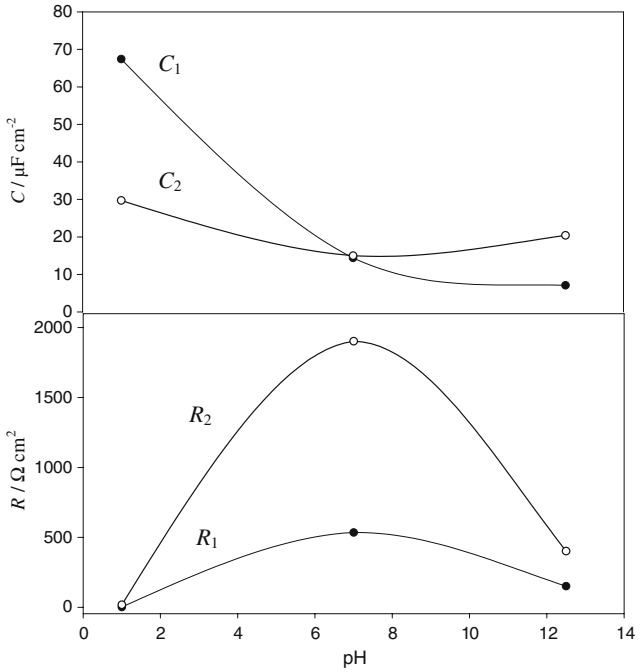

Fig. 7 The two capacitive elements C_1 and C_2 for the outer and inner layers of the surface film on AZ91D alloy and their two resistive elements R_1 and R_2, in 0.1 M Na_2SO_4 solution of various pH

simulate the recorded impedance diagrams. Over this time domain, the impedance trend is to decrease with the testing period where a localized corrosion and pitting are evident. The proposed model (Fig. 8c) consists from (R_1CPE$_1$) parallel combination representing the corroded area (pit) parallel connected with the time constant (R_2CPE$_2$) of the protected area [4, 24] (Fig. 8c). By this way, the first time constant at LF region originates from the charge-transfer resistance (R_{ct}) and the double layer capacitance (C_{dl}) at the actively corroding areas, while the second at HF region pertains to the corrosion product film (R_fC_f) on the passive zones. To compensate the error arising from surface roughness, CPEs were considered in the EC. The circuit parameters shown in Table 4b indicate that for long immersion term the gradual decrease in the resistance (R_{ct}) of the corroding area (pit site) with time is likely due to an increase in the corrosion rate of AZ91D, as will be seen later in the polarization results. Also, accumulation of the corrosion debris in the pitting zone would modify the conductivity for charge transfer and thus decreases its resistance. Meanwhile, the decrease in the resistance (R_f) on the protected area with time may be the result of formation of small pores or micro cracks in the surface layer. Alternatively, this may result from the slow thinning of the MgO surface layer due to the reaction between MgO and water at the bottoms of the pores. Therefore, the resulting volume expansion at the bottoms of the pores could, in turn, cause further cracking in the surface film, thereby decreases the alloy stability with immersion in solution. However, the capacitance of the corroding sites (C_{dl}) is relatively higher compared with that for the protected non-degraded zone.

Figure 9 shows the time dependence of the surface film resistance (R_f) and its relative thickness ($1/C_f$) up to 500 h. As can be seen, the trends of $1/C_f$ are mirrored completely by those of R_f. Based on these results, the alloy would be highly stable and protected only over short exposure times up to ~50 h. Over these intervals, the resistance and thickness of the corrosion product films increase sharply and linearly with time. After, surface film stability is reduced with immersion, when localized attack and pit nucleation start to initiate causing film failure with a subsequent decrease in R_f and $1/C_f$ values. This behavior clearly indicates film disruption and dissolution due to enhanced corrosion. Also, it seems that thinning of the surface film proceeds through a dissolution–precipitation mechanism [16, 17, 25], since both R_f and $1/C_f$ become time-independent when the alloy immersion is prolonged for more than 400 h. At this time, the surface film attains a steady state thickness and resistance. It is noteworthy that following 100 up to 500 h immersion, the color of the surface film gradually changes from faint gray to deep gray, especially at the sample edge of the exposed area. Appearance of some darker small spots on the surface is also seen after 500 h immersion time, where the evolution of H_2 bubbles are mostly limited to those spots on the sample area. Therefore, any newly formed $Mg(OH)_2$ is likely generated from the chemical reaction between MgO at the base of the pores layer and water, and not from a corrosion reaction between Mg in the substrate and water or even oxygen [26].

Potentiodynamic behavior

Effect of SO_4^{2-} concentration

Figure 10a shows linear sweep potentiodynamic traces for AZ91D alloy in Na_2SO_4 solutions (0.01–1.0 M) at a scan rate of 1 mV s^{-1} over the range −2.0 to −0.5 V vs. SCE. These scans enable the determination of various electrochemical corrosion parameters of the alloy using Thales software for *i*/*E* analysis [16, 17, 27]. The corrosion current density (i_{corr}) was determined from the intersection of the cathodic Tafel line, −50 mV from E_{corr}. In general, as SO_4^{2-} concentration increases the shape of the polarization curves remains similar with a progressive increase in the current and gradual shift to more active potentials, indicating simultaneous activation promotion for cathodic and anodic reactions. The cathodic curves exhibit a well-defined Tafel behavior over a large potential range corresponding to water reduction via the reaction: $2H_2O + 2e = H_2 + 2OH^-$, as has been previously

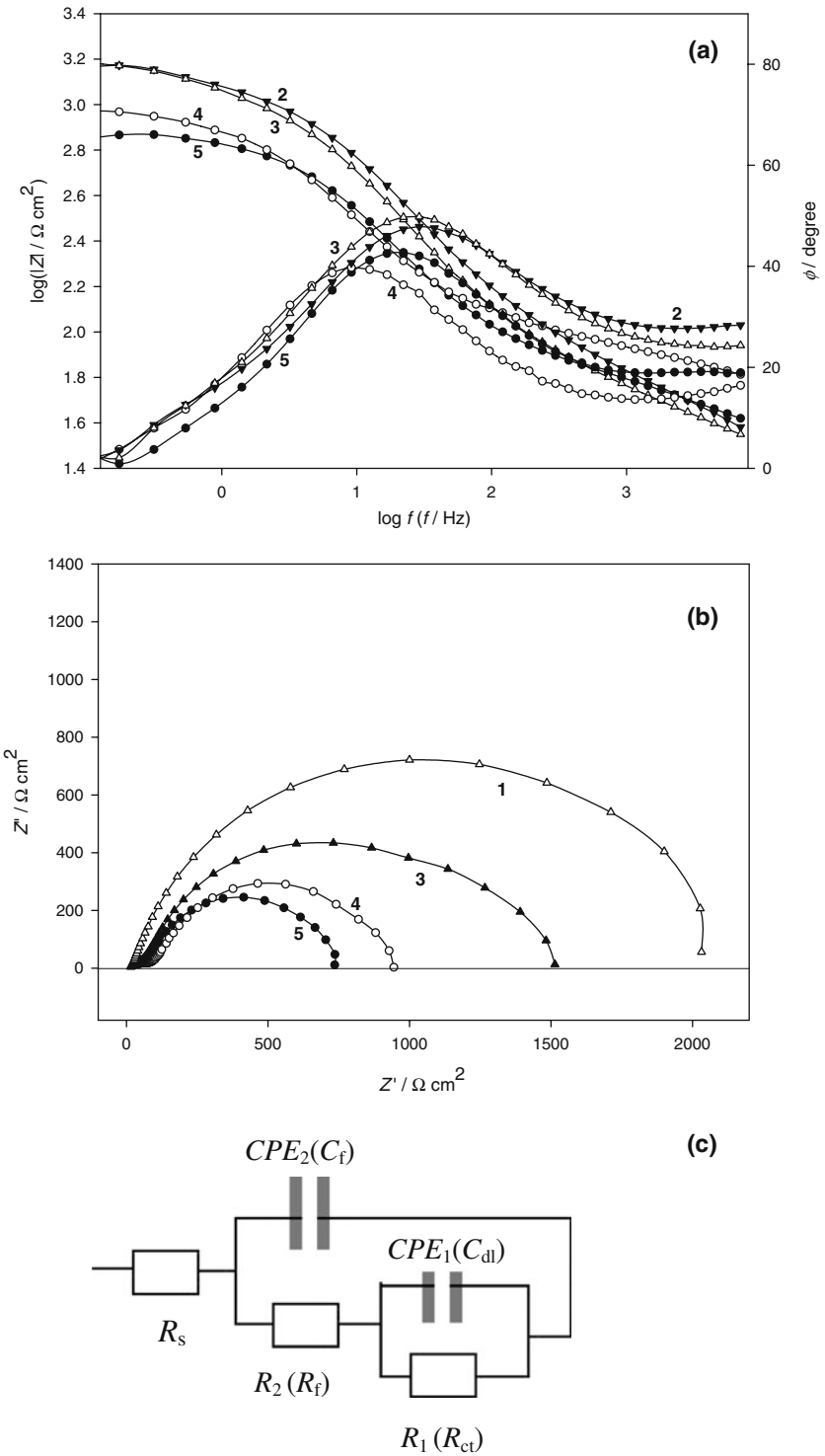

Fig. 8 The EIS data for AZ91D alloy in 0.1 M Na_2SO_4 solution after various long immersion times: (*1*) 100 h, (*2*) 200 h, (*3*) 300 h, (*4*) 400 h, and (*5*) 500 h. **a** The Bode plots, **b** the Nyquist plots, and **c** the equivalent circuit used to fit these data

reported [28]. On the other hand, the anodic scans reveal a sharp increase in the polarizing current density over a narrow potential range after E_{corr}, followed by a current plateau bounded by E_{corr} and the pitting potential (E_{pit}), whose range decreases with increasing concentration. The current plateau indicates the existence of some partially protective film, namely $Mg(OH)_2$, on the alloy surface [8]. Indeed, this plateau has too-high current density values (50–250 μA cm^{-2}) to be suggested as a true passivating layer [28]. Hence, it can be assumed that the alloy remains in a pseudo-passive state over the potential range of the current plateau. At E_{pit}, the surface film suffers local breakdown accompanied by a noticeable hydrogen gas evolution and the current growth rate becomes higher when the potential exceeds E_{pit}. Over

Table 4 Equivalent circuit parameters of AZ91D alloy immersion in naturally aerated 0.1 M Na_2SO_4 solution for: (a) short times from 15 min to 48 h and (b) long times from 100 h; at 298 K

time (h)	R_s (Ω cm^2)	R_1 (Ω cm^2)	C_1 (μF cm^{-2})	R_2 (kΩ cm^2)	C_2 (μF cm^{-2})	ϕ_{max} (degree)	$1/C_f$ (μF^{-1} cm^2)
a							
15 min	11.8	526	7.64	0.85	35.34	60.2	0.16
30 min	9.63	883	7.60	1.30	22.83	64.0	0.18
1	11.2	985	8.40	1.68	19.51	67.9	0.17
2	11.7	535	14.42	1.90	15.01	67.7	0.14
3	9.41	674	19.75	1.91	7.60	67.7	0.18
6	11.8	792	11.41	2.46	6.55	67.7	0.24
12	10.7	676	13.71	2.49	6.40	67.2	0.23
24	12.7	734	14.61	2.51	6.30	66.2	0.23
48	13.1	698	14.85	2.63	5.55	62.7	0.25
b							
100	67	94.4	4.44	1.97	4.14	52.4	0.24
200	77	90.8	7.43	1.36	5.69	47.8	0.18
300	98	61.5	9.18	1.15	7.44	49.8	0.13
400	138	54.4	17.05	0.65	14.62	42.7	0.07
500	201	49.9	20.02	0.60	17.20	39.7	0.06

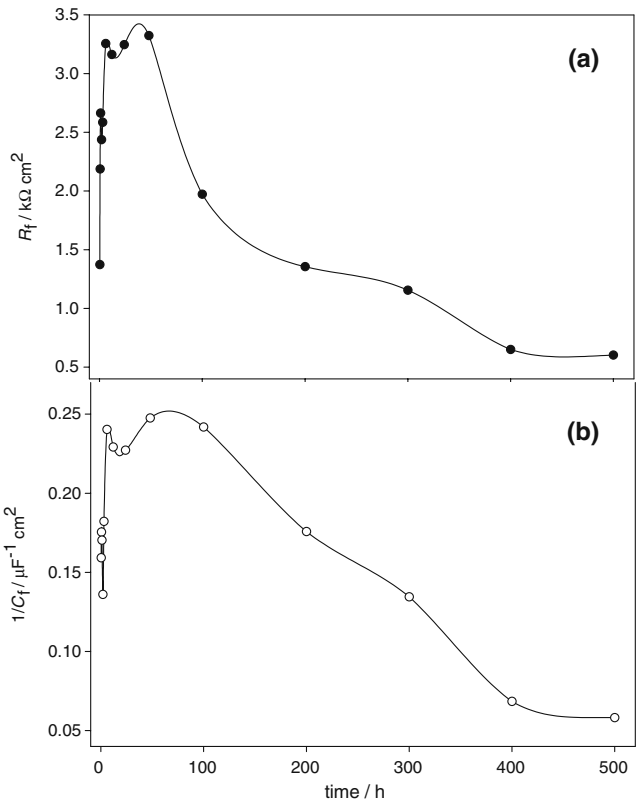

Fig. 9 Development of the surface film **a** resistance and **b** its relative thickness with time for AZ91D alloy immersed in naturally aerated 0.1 M Na_2SO_4 solution at 298 K

this polarization range, SO_4^{2-} anions acts aggressively towards AZ91D causing localized corrosion and pitting propagation occurs with a rapid increase in the current. The corrosion parameters (i_{corr}, E_{corr}, and E_{pit}) are also given in Table 1.

Variation of corrosion current density (i_{corr}) and pitting potential (E_{pit}) are depicted in Fig. 10b as a function of SO_4^{2-} concentration. It is obvious that i_{corr} increases, while E_{pit} changes negatively with increasing concentration quickly at first and then slowly. This behavior is in good agreement with the EIS results and indicates that the aggressive nature of SO_4^{2-} anions is more pronounced in the more dilute solutions. A result which fulfills Brasher's theory [29] on the role of anions in promoting or inhibiting corrosion depending on their type and concentration.

Effect of temperature

All measured polarization curves over the temperature domain 278–338 K exhibit comparable behavior suggesting similar reactions at the alloy surface. The anodic active dissolution rate of the alloy increases exponentially until reaching the pseudo-passive potential zone characterized by a current plateau, whose range tends to be wider with decreasing temperature. However, at E_{pit}, depassivation sets up and the rate of anodic dissolution deviates to higher current densities commensurate with a vigorous hydrogen gas evolution, especially at higher temperatures. This behavior evinces that lower temperatures are in favor of forming and maintaining better protective film on the alloy surface. Meanwhile, the rate of cathodic hydrogen evolu-

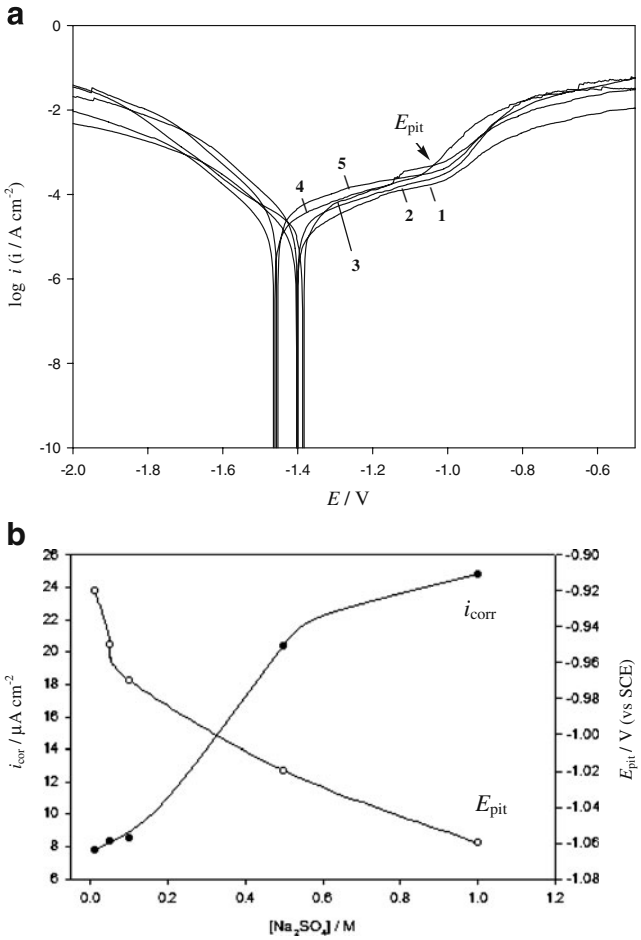

Fig. 10 **a** Cathodic and anodic scans of AZ91D alloy in Na_2SO_4 solutions of different concentrations: (*1*) 0.01 M, (*2*) 0.05 M, (*3*) 0.1 M, (*4*) 0.5 M, and (*5*) 1.0 M. **b** Dependence of i_{corr} and E_{pit} for AZ91D alloy on Na_2SO_4 concentration at 298 K

tion through water reduction, which develops more easily on film-free areas of AZ91D surface, remarkably decreases with lowering temperature.

Moreover, the results clearly show that temperature promotes the rapid attack of AZ91D alloy in neutral sulfate solution as substantiated from the increase in the corrosion current density (i_{corr}) as well as the shift of E_{corr} and E_{pit} towards more negative potential values (Table 2). The linear relationship between log i_{corr} and $1/T$, shown in Fig. 11, indicates that the corrosion reaction of AZ91D can be regarded as Arrhenius-type process, the rate of which is given by: i_{corr} = constant exp ($-E_a/RT$). From the slope of this plot ($-E_a/2.303R$, R being the gas constant) the calculated value of the apparent activation energy (E_a) was found equal to 28.5 kJ mol^{-1}. This value is somewhat higher than the corresponding one for AZ91D in chloride medium and less than those in bromide and iodide solutions [17]. The comparison confirms that although SO_4^{2-} is less aggressive than Cl^-, it is rather more corrosive than Br^- or I^- ions. Thus, sulfate solution is considered to moderately promote AZ91D corrosion particularly at higher temperatures.

Effect of pH

Figure 12a shows polarization scans of AZ91D samples in 0.1 M Na_2SO_4 solutions of various pH. The cathodic Tafel line at pH 12.5 has lower current densities than those in pH 7.0 or 1.0, suggesting that the rate of HER on AZ91D surface is much faster in acidic and neutral solutions than in the alkaline. On the other hand, the anodic scans reveal that although the wider passive current plateau exists in pH 12.5, the lowest pseudo-passive current density (i_p) is obtained in pH 7.0 and the highest in pH 1.0. This confirms a quite-higher propensity of the neutral sulfate medium to form and sustain better protective anodic film on the alloy surface, albeit over a narrow potential range bounded by E_{corr} and the vigorous attack at the arrow because of more corrosion. For alkaline solution, the arrow indicates corrosion rate increase after a long relatively passive plateau. In fact, this discrepancy of more active breakdown potential for neutral than for alkaline solution suggests different mechanism to explain the negative difference effect (NDE), which associates the excessive hydrogen evolution at and beyond E_{pit} [17, 30]. Thus, in alkaline solution, this is likely to be in terms of undermining and falling away of the β-phase particles under high anodic polarization [24]. While in acidic and neutral solutions, the NDE is most probable due to breakdown of the partially protective film on the alloy surface [30].

The electrochemical corrosion parameters cited in Table 3 obviously show that both i_{corr} and i_p exhibit similar trend. Hence, the corrosion behavior of AZ91D alloy can be envisaged based on how its micro-constituents interact when it is exposed to media with various pH. In highly acidic conditions, the observed very high i_{corr} value

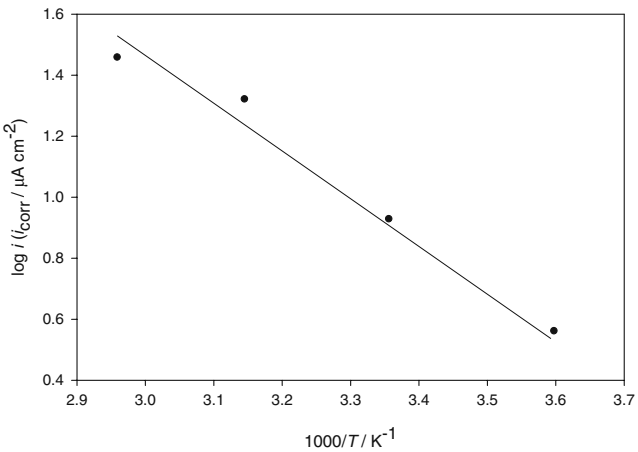

Fig. 11 Arrhenius plot for the corrosion process of AZ91D alloy in 0.1 M Na_2SO_4 solution

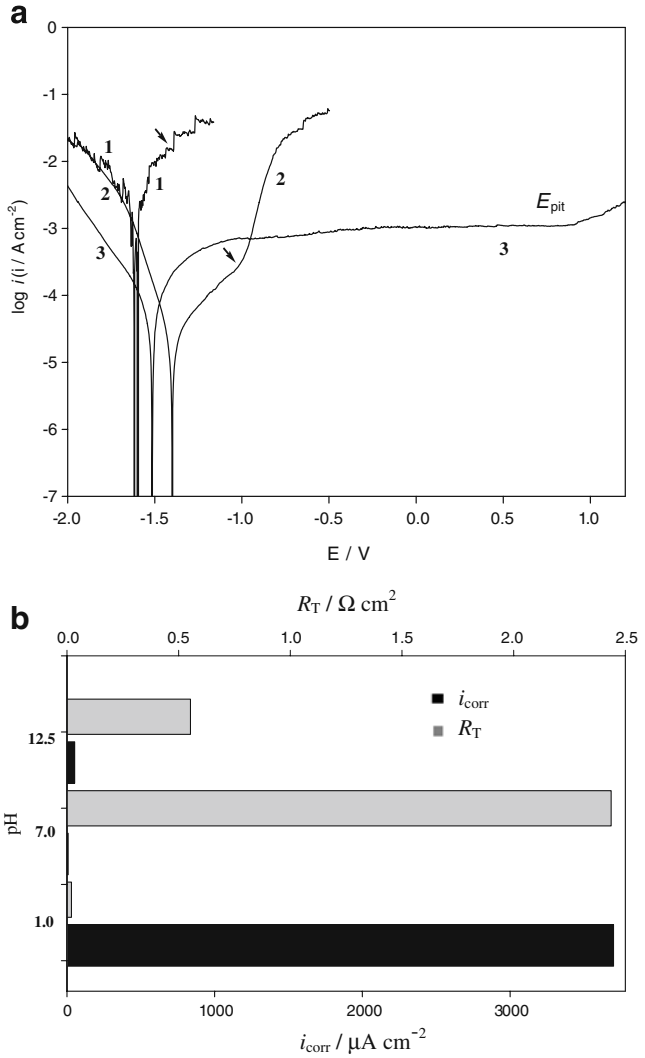

Fig. 12 **a** Potentiodynamic cathodic and anodic polarization scans for AZ91D alloy in 0.1 M Na_2SO_4 solution of various pH: (*1*) 1.0, (*2*) 7.0, and (*3*) 12.5. **b** Dependence of R_T and i_{corr} of AZ91D alloy on the pH of naturally aerated 0.1 M Na_2SO_4 solution at 298 K

(3.7 mA cm^{-2}) suggests general corrosion attack as the main mechanism of degradation. However, in neutral solution, corrosion occurs in the grain body due to galvanic coupling between the α-Mg matrix and the eutectic areas surrounding the β-phase, as these zones are comparatively cathodic. Since polarization test did not show a clearly defined pitting potential, so the corrosion process should be associated with a localized attack, but not a typical pitting attack. The lower corrosion rate (8.5 μA cm^{-2}) and the better passivation of AZ91D at these conditions owe to fine

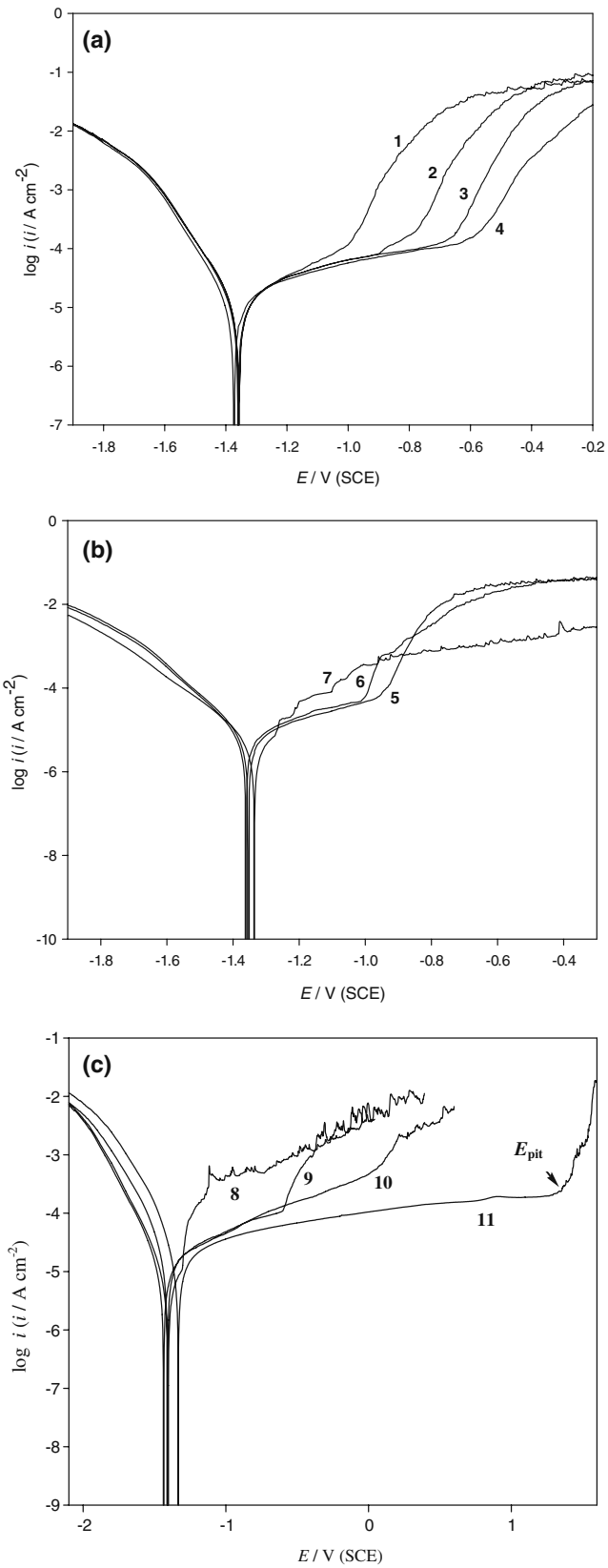

Fig. 13 **a**–**c** Potentiodynamic cathodic and anodic polarization scans for AZ91D alloy measured after immersion in 0.1 M Na_2SO_4 solution for various time intervals: **a** *1* (15 min), *2* (30 min), *3* (1.0 h), and *4* (3.0 h). **b** *5* (6.0 h), *6* (12 h), and *7* (100 h). **c** *8* (200 h), *9* (300 h), *10* (400 h), and *11* (500 h)

distribution of β-phase with the eutectic α-phase at the interface. It is expected that the film formed on the α-eutectic and β-phase is more stable because of the presence of higher amount of aluminum [31]. The continuous stable oxide film acts as a barrier so that the dissolution of α-phase is inhibited.

Furthermore, in alkaline pH, Al dissolution will be much higher than that of Mg. Therefore, the α-eutectic phase mixture can be expected as preferentially attacked region in AZ91D alloy at pH 12.5. In this case, the grain interiors will be un-attacked and the dissolution of the alloy will be mainly in the eutectic areas, located at the grain boundaries. The increase in i_{corr} value (52.5 μA cm^{-2}) than that in the neutral solution may result from this intergranular corrosion [32]. The first stage of corrosion of the eutectic areas occurs by galvanic coupling with the nobler β-phase, and the β-phase could deteriorate when the corrosion of the α-eutectic phase is sufficient. It is also noteworthy that formation of corrosion products on the grain body decreases the galvanic effects between the grain and the surroundings. Figure 12b shows clearly that the inverse trend of i_{corr} is mirrored completely by the trend of the total resistance (R_T) of the surface film on the alloy at various pH, which indicates good agreement between dc and ac results.

Effect of testing time

As can be seen in Fig. 13a–c, at all tested times from the shortest (15 min) to the longest (500 h) each polarization curve is characterized by a much steeper anodic branch in the active dissolution region than the cathodic branch. It is also obvious that corrosion product films formed spontaneously on AZ91D surface after various exposure periods have no influence on the cathodic branch, which refers to the cathodic hydrogen evolution via water reduction [9, 28]. While those films that do influence the corrosion rate and the passive behavior, as well as the breakdown potential (E_{pit}) on the anodic branch, are most likely due to surface modifications that occur during immersion.

Based on Fig. 14, the effect of immersion time on the corrosion behavior of AZ91D alloy may be explained as follows. For the first initial exposure times (15 min–3 h), i_{corr} decreases sharply and linearly, in conformity with the sharp and linear increase of E_{corr} to more positive potential values. During the earlier stage, the formed protective films play an important role in the corrosion process and stability of the alloy. It may be assumed that the film-covered area (θ) on AZ91D surface rapidly increases with time and the film-free area ($1-\theta$) decreases leading to a continuous fast decrease in the corrosion rate of the alloy. Parallel to that, the passive current decreases and its potential range increased; in the meanwhile the surface film resistance to local breakdown under anodic polarization is clearly improved as indicated by the noticeable shift of E_{pit} towards more positive potential values (Fig. 13a). This would suggest a uniform corrosion attack over the first initial hours of immersion, and reveals that spontaneous corrosion product films formed during the short-term exposure have protective ability that enhance the alloy resistance against the attack by the corrosive SO_4^{2-} species. For intermediate immersion times (6–48 h), the growth rates and consequently thicknesses of the surface films would be crucial factors leading to a much small decrease in i_{corr} with a simultaneous re-increase in the negative value of E_{pit} (Fig. 13b). It is noteworthy to indicate that at most of those testing times, the anodic current in the pseudo-passive range suffers from clear oscillations which make the breakdown potential difficult to be correctly detected. Upon longer exposure of more than 48 h, Fig. 14 reveals gradual increase in i_{corr} with time, implying a decrease in the stability of the corrosion product film on the alloy due to its dissolution, leading to an increase in the corrosion

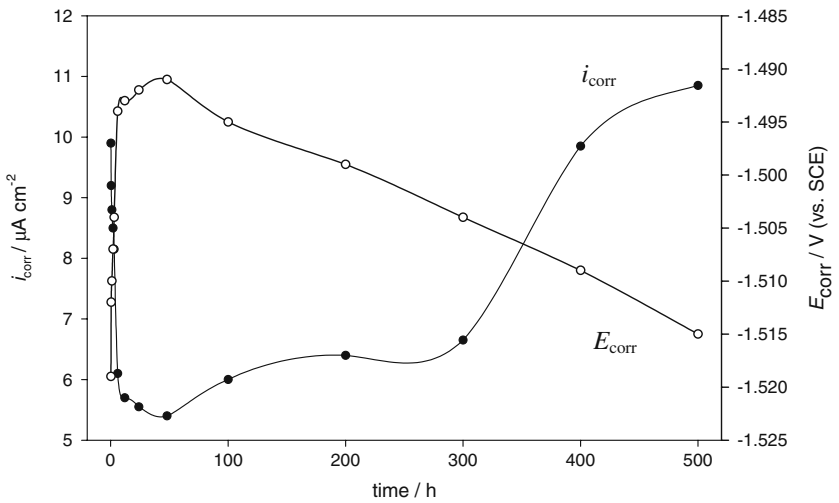

Fig. 14 Dependence of the corrosion parameters i_{corr} and E_{corr} for AZ91D alloy on the open-circuit exposure period in naturally aerated 0.1 M Na_2SO_4 solution at 298 K

vulnerability of the alloy. This behavior is also confirmed by the negative drift of E_{corr} to more active potential values.

Due to the heterogeneous microstructure of AZ91D alloy, the mode of attack by which its corrosion proceeds during the extended immersion should be varied. By considering the Al contents in the three main phases constituting the microstructure of AZ91D surface [4], it is obvious that spreading out the corrosion attack to the eutectic area during the long-term immersion produces corrosion product layers strongly enriched with aluminum [15]. The Al enrichment in the corrosion products film greatly increases the alloy resistance to passivity breakdown under anodic polarization, which in this case occurs through undermining and falling away of the β-phase particles, rather than by the breakdown of the partially protective film [24]. In fact, this could explain the significant shifts in E_{pit} to more positive potential values with prolonging the exposure period, as shown by curve 11 in Fig. 13c for AZ91D sample immersed 500 h in the test solution.

Conclusion

Various electrochemical techniques were used to examine the effects of some experimental factors on the behavior of AZ91D alloy in aqueous sulfate medium. The following are the most important findings drawn from the present study.

1. Both of the corrosion and pitting potentials (E_{corr} and E_{pit}) of AZ91D alloy were found to decrease (become more active) with increasing concentration and temperature of the test solution, while i_{corr} increases indicating a decrease in the stability of the partially protective film on the alloy surface.
2. Neutral sulfate solution (pH 7.0) supports the formation of a better protective layer on AZ91D alloy than alkaline (pH 12.5) or acidic (pH 1.0) one.
3. The alloy exhibits enhanced stability during open-circuit exposure for short times up to ~50 h, where each of E_{corr}, R_f or $1/C_f$ parameter for the corrosion products film increases with time, while i_{corr} decreases. However, for longer exposure up to 500 h, E_{corr} drifts negatively again and i_{corr} increases due to breakdown of the protective film and a decrease in its resistance and thickness.
4. Fitting the impedance data to the appropriate equivalent circuit model helps to confirm the mode of corrosion attack occurring during open-circuit exposure.

References

1. Watarai H, January (2006) “Science & Technology Trends”, Quarterly Review No. 18
2. Kainer KV (2003) Magnesium—alloys and technology. Wiley-VCH. KG aA, Weinheim
3. Chen J, Wang J, Han E, Dong J, Ke W (2007) Electrochim Acta 52:3299
4. Baril G, Blanc C, Keddam M, Pébère N (2003) J Electrochem Soc 150:B488
5. Pilling N, Bedworth R (1923) J Inst Met 29:529
6. Hoey GR, Cohen M (1959) J Electrochem Soc 106:776
7. Hara N, Kobayashi Y, Kagaya D, Akao N (2007) Corros Sci 49:166
8. Wu G, Fan Y, Atrens A, Zhai C, Ding W (2008) J Appl Electrochem 38:251
9. Ambat R, Aung NN, Zhou W (2000) J Appl Electrochem 30:865
10. Inoue H, Sugahara K, Yamamoto A, Tsubakino H (2002) Corros Sci 44:603
11. Pardo A, Merino MC, Coy AE, Arrabal R, Viejo F, Matykina E (2008) Corros Sci 50:823
12. Pébère N, Riera C, Dabosi F (1990) Electrochim Acta 35:555
13. Chen J, Wang J, Han E, Dong J, Ke W (2005) Mater Corros 57:789
14. Baril G, Pébère N (2001) Corros Sci 43:471
15. Baril G, Blanc C, Pébère N (2001) J Electrochem Soc 148:B489
16. Heakal FET, Fekry AM, Fatayerji MZ (2009) J Appl Electrochem 39:583
17. Heakal FET, Fekry AM, Fatayerji MZ (2009) Electrochim Acta 54:1545
18. Pourbaix M, “Atlas of electrochemical equilibria in aqueous solutions”, (1974) National Association of Corrosion Engineers (NACE), pp 136–145 and pp 168–176
19. Jüntter K (1990) Electrochim Acta 35:1501
20. Macdonald JR (1987) Impedance spectroscopy, 3rd edn. Wiley, New York
21. Rammelt U, Reinhard G (1990) Electrochim Acta 35:1045
22. Heakal FET, Fekry AM (2008) J Electrochem Soc 155:C534
23. Mansfeld F, Kendig MW (1988) J Electrochem Soc 135:828
24. Guo X-W, Chang J-W, He S-M, Ding W-J, Wang X (2007) Electrochim Acta 52:2570
25. Ismail KM, Virtanen S (2007) Electrochem Solid-state Lett 10:C9
26. Xia SJ, Yue R, Rateick RG Jr, Birss VI (2004) J Electrochem Soc 151:B179
27. Heakal FET, Fekry AM, Ghoneim AA (2008) Corros Sci 50:1618
28. Bedjoudi T, Fiaud C, Robbiola L (1993) Corrosion 49:738
29. Brasher DM (1962) Nature 193:868
30. Song G, Atrens A, Wu X, Zhang B (1998) Corros Sci 39:1769
31. Ambat R, Aung NN, Zhou W (2000) Corros Sci 42:1433
32. Anik M, Avci P, Tanverdi A, Celikyurek I, Baksan B, Gurler R (2006) Mater Des 27:347